SIMPLIFIED ANALYTICAL SOLUTIONS FOR MAGNETIC STIMULATION OF NEURONS

Karu P. Esselle† *and* **Maria A. Stuchly** ‡

† Bureau of Radiation and Medical Devices
Health and Welfare Canada
Room 225, 775 Brookfield Road, Ottawa, ON, K1A 1C1, Canada
‡ Dept. of Electrical and Computer Engineering
University of Victoria
P.O. Box 3055, Victoria, B.C., V8W 3P6, Canada[1)]

ABSTRACT

Strong pulses of magnetic field are used to stimulate peripheral nerves and motor neurons in the cerebral cortex. Such stimulation is used in neurology for numerous diagnostic purposes. The electric field induced in tissue along the neuron and its spatial derivative are the parameters determining neural response. Another important parameter influencing the efficiency of stimulation is the inductance of a coil producing the magnetic field, as it defines the current time derivative for a given pulse generator. For arbitrarily located coils of arbitrary shapes, a semi-analytical solution is presented to calculate spatial distributions of the electric field and its spatial derivatives in a semi-infinite tissue model. Analytical solutions are given for coils composed of linear segments parallel or perpendicular to the air-tissue interface. Expressions for inductance of coils having suitable geometries for neural stimulation are derived. Coils can be optimized for stimulation of nerves at given orientation and distance from the air-tissue interface. In the optimization, coil dimensions and shape are considered as they affect both the induced field and inductance. A quadruple coil consisting of triangular sections appears to offer some advantages over other shapes for stimulation of shallow nerves. For deep nerves spaced quadruple square and three-dimensional coils are preferred. Analyses described are useful in evaluating various options, gaining an insight into the physical phenomena involved, and as the first step before undertaking a numerical analysis of models more closely representing the tissue electrical and geometrical complexities.

I. INTRODUCTION

Since the mid-1980s magnetic stimulation of neurons has gained rapid acceptance as a diagnostic and research tool in neurology [Geddes, 1991]. Various medical conditions associated with abnormal conduction in motor pathways can be diagnosed by stimulating an appropriate neuron and measuring the conduction velocity by recording motor action potentials. Diseases such as multiple sclerosis, cervical myelopathy, myelopathy, cerebral palsy, Bell's palsy and others can be diagnosed [Barker *et al.*, 1986, 1987, Chokroverty, 1990, Maccabee *et al.*, 1991, Murray, 1991]. Mapping of the motor cortex has been used to evaluate congenital mirror movements, amputations, spinal cord injury and effects of hemispherectomy [Cohen *et al.*, 1991].

Neural stimulation occurs when an externally applied stimulus has a sufficient amplitude and duration to cause current to flow through a cellular (neural) membrane and change its potential above a threshold value. In case of magnetic stimulation the stimulus is produced by a pulse of magnetic field from an external coil. The electric field induced in tissue is proportional to the time derivative of the coil current. For overdamped current pulses, which are preferred in neural stimulation, the current derivative is [Basser and Roth, 1991]:

$$\frac{dI(t)}{dt} = \frac{V}{L} e^{-\omega_1 t} \left[\cosh(\omega_0 t) - \frac{\omega_0}{\omega_1} \sinh(\omega_0 t)\right] \qquad (1)$$

1) This work was performed at the Bureau of Radiation and Medical Devices, Health and Welfare Canada.

where V is the voltage, L is the coil inductance, $\omega_1=R/2L$, R is the series resistance, and

$$\omega_0 = \left[\left(\frac{R}{2L}\right)^2 - \frac{1}{LC}\right]^{1/2}$$

where C is the capacitance of the stimulator capacitor charged to voltage V, which then is discharged through the coil. This relationship indicates that for a given generator (V and C), the stimulus (at $t=0$) is inversely proportional to the inductance.

For long nerves, the sub-threshold transmembrane potential can be derived from a passive cable equation, and for magnetic stimulation it takes the following form [Basser and Roth, 1991]:

$$\lambda_0^2 \frac{\partial^2 V_m}{\partial x^2} - \tau_0 \frac{\partial V_m}{\partial t} - (V_m - V_r) = \lambda_0^2 \frac{\partial E_x}{\partial x} \qquad (2)$$

where V_m is the transmembrane potential, V_r is the resting potential, λ_0 is the neural space constant, τ_0 is the neural time constant, E_x is the electric field strength along x, *i.e.* the direction of the neuron.

The electric field spatial derivative $\partial E_x/\partial x$, also referred to as the activating function, therefore plays an important role in magnetic nerve stimulation. Depending on the sign of the activation function, the neuron is either depolarized (negative derivative) or hyperpolarized. All neurons that are depolarized above a threshold level (determined by nerve size, pulse width, *etc.*) are stimulated. Equation (2) and these considerations apply directly to long, straight axons; the situation is more complex in case of short neurons with dendrites and it is likely that both the electric field and its derivative will be important.

The importance of evaluation of the induced electric field and its derivatives is apparent. Furthermore, various coil geometries and orientations can produce vastly different spatial distributions of the fields. A simplified analysis of induced fields using an analytical method was previously performed, but the charge accumulation on the air-tissue interface was neglected [Grandori and Ravazzani, 1991]. Numerical techniques were used to analyze homogeneous and layered tissue models such as a semi-infinite tissue space [Roth *et al.*, 1990a], cylinder [Roth *et al.*, 1990a] and sphere [Branston and Tofts, 1991, Roth *et al.*, 1991a]. The numerical analyses performed so far require a considerable computing time, of the order of hours, and large memories, yet do not account for tissue heterogeneity. Another limitation of these methods is that physical insight is lost, hindering their use for optimization or improvement of the coil geometry.

We have previously derived analytical expressions for the induced electric field and its spatial derivatives in a semi-infinite tissue half-space produced by a very short element of current-carrying coil [Esselle and Stuchly, 1992]. Using this method it is possible to calculate within minutes using a microcomputer the induced fields from an arbitrarily shaped and oriented coil. In this contribution we further extend this method and develop closed-form expressions for coils consisting of linear segments of wire parallel or perpendicular to the air-tissue interface. Methods are developed to calculate the inductance of such coils. The coil size is optimized to obtain the strongest stimulus at a given depth. Three promising coil configurations: quadruple square coil (QS), quadruple triangular coil (QT) and three-dimensional (3D) coil are described, analyzed and compared. Performance of these coils is evaluated by considering the following criteria: the strength of the peak stimulus for a given voltage, the rate at which the peak stimulus decreases with depth, the peak hyperpolarization level as a fraction of the peak depolarization level, and the size of the stimulation region (spot).

II. CALCULATION OF INDUCED ELECTRIC FIELD

Infinitesimal Coil Element

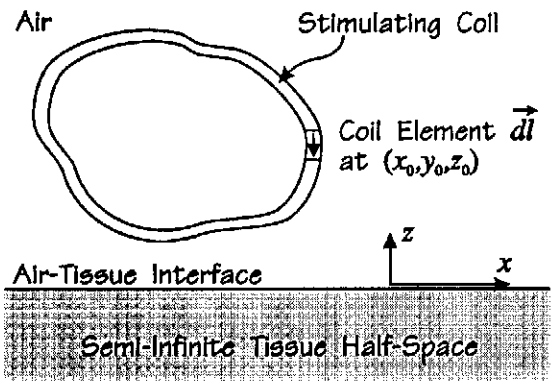

Figure 1. A stimulating coil of arbitrary shape, above a semi-infinite tissue block.

The computation of the induced electric field in the semi-infinite tissue half-space, shown in Fig. 1, from a time-varying current in an external, arbitrarily-shaped coil usually requires several numerical steps. However the electric field from an infinitesimal element of the coil can be evaluated analytically [Esselle and Stuchly, 1992], provided that the time-variation of current is slow enough to justify quasi-static approximations [Roth *et al.*, 1991b]. For a coordinate system with its origin on the interface and z-axis perpendicular to the interface, and for a tissue half-space homogeneous in the x- and y-directions, the quasi-static electric field components induced at point (x,y,z) in tissue by a coil-element $\vec{dl}$ located at (x_0, y_0, z_0) in free-space are as follows [Esselle and Stuchly, 1992]:

$$dE_x = -\frac{\mu_0(dI/dt)}{4\pi}\left\{\frac{dl_x}{R}+\frac{dl_z(x-x_0)}{\rho^2}\left(1+\frac{z-z_0}{R}\right)\right\} \tag{3}$$

$$dE_y = -\frac{\mu_0(dI/dt)}{4\pi}\left\{\frac{dl_y}{R}+\frac{dl_z(y-y_0)}{\rho^2}\left(1+\frac{z-z_0}{R}\right)\right\} \tag{4}$$

$$dE_z = 0 \tag{5}$$

where

$$\rho = \sqrt{(x-x_0)^2+(y-y_0)^2}, \tag{6}$$

$$R = \sqrt{(x-x_0)^2+(y-y_0)^2+(z-z_0)^2}, \tag{7}$$

dl_x, dl_y and dl_z are the components of the vector $\vec{dl}$, μ_0 is the permeability of free space (4π x 10^{-7} H/m) and dI/dt is the time rate of change of coil current. The induced current is given by $\vec{J}=\sigma\vec{E}$ where σ is tissue conductivity. The spatial derivatives of the induced electric field components are given by:

$$d\left(\frac{\partial E_x}{\partial x}\right) = \frac{\mu_0(dI/dt)}{4\pi}\left\{\frac{(x-x_0)\,dl_x}{R^3}+\left[\frac{(x-x_0)^2-(y-y_0)^2}{\rho^4}\right]dl_z+\left[\frac{(x-x_0)^2-(y-y_0)^2}{R\rho^4}+\frac{(x-x_0)^2}{\rho^2R^3}\right](z-z_0)\,dl_z\right\} \tag{8}$$

$$d\left(\frac{\partial E_y}{\partial y}\right) = \frac{\mu_0(dI/dt)}{4\pi}\left\{\frac{(y-y_0)\,dl_y}{R^3}+\left[\frac{(y-y_0)^2-(x-x_0)^2}{\rho^4}\right]dl_z+\left[\frac{(y-y_0)^2-(x-x_0)^2}{R\rho^4}+\frac{(y-y_0)^2}{\rho^2R^3}\right](z-z_0)\,dl_z\right\} \tag{9}$$

The total electric field and the spatial derivatives can be obtained by integrating numerically the corresponding

expression along the length of the coil. This method of field computation is more efficient than methods used previously, since the numerical computation used here is very simple and requires little time.

It is interesting to note that neither the electric field nor its spatial derivatives depend on tissue conductivity σ. This is a result of the following quasi-static assumptions made in the derivation: (1) tissue is a good conductor where the displacement current is negligible compared with the conduction current ($\sigma >> 2\pi f\epsilon$), (2) tissue is not an excellent conductor, and therefore, the skin depth ($1/\sqrt{(\mu\sigma\pi f)}$) is much larger than the system dimensions. At sufficiently low frequencies (< 10 kHz), these conditions are valid for most biological tissues [1991a]. As long as the tissue behaves as a good-but-not-excellent conductor, the induced electric field is independent of its conductivity and permittivity.

Linear Coil Segment Parallel to the Interface

Most of the best-performing stimulating coils, such as double and quadruple square coils, are composed of several linear segments [Esselle and Stuchly, 1992]. Others, such as circular coils, can be approximated by polygon-shaped coils composed of linear segments [Cohen *et al.*, 1990]. In these cases, the fields and their spatial derivatives produced by each linear segment can be evaluated analytically saving considerable amounts of computer time, and allowing for physical insight.

Let us consider a linear segment of a coil parallel to the interface and extending from (x_1, y_1, z_0) to (x_2, y_2, z_0). The projection of the segment on the x-y plane is shown in Fig. 2, together with the projection of the point (x,y,z) where the field is evaluated. The electric field components produced by the segment can be obtained by integrating expressions (3) and (4) along the length of the segment. Analytical integrations result in the following expressions:

$$E_x = \frac{\mu_0 (dI/dt)}{4\pi}\left[\sinh^{-1}(\cot\alpha_2) - \sinh^{-1}(\cot\alpha_1)\right]\cos\theta \tag{10}$$

$$E_y = \frac{\mu_0 (dI/dt)}{4\pi}\left[\sinh^{-1}(\cot\alpha_2) - \sinh^{-1}(\cot\alpha_1)\right]\sin\theta \tag{11}$$

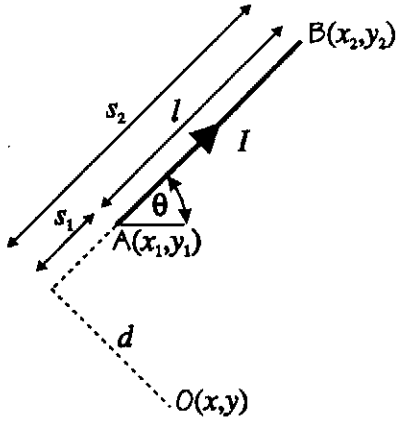

Figure 2. The projection of a linear segment parallel to the interface on the x-y plane. The projection of the point where the fields are calculated is also shown (O).

where $$\alpha_1 = \cos^{-1}\left[\frac{(x_1-x)(x_1-x_2)+(y_1-y)(y_1-y_2)}{R_1 l}\right] \tag{12}$$

$$\alpha_2 = \cos^{-1}\left[\frac{(x_2-x)(x_1-x_2)+(y_2-y)(y_1-y_2)}{R_2 l}\right] \tag{13}$$

$$R_1 = \sqrt{(x-x_1)^2+(y-y_1)^2+(z-z_0)^2} \tag{14}$$

$$R_2 = \sqrt{(x-x_2)^2+(y-y_2)^2+(z-z_0)^2} \tag{15}$$

$$l = \sqrt{(x_1-x_2)^2+(y_1-y_2)^2} \tag{16}$$

and $$\theta = \tan^{-1}\left(\frac{y_2-y_1}{x_2-x_1}\right). \tag{17}$$

The spatial derivatives of the electric field due to the linear

parallel segment can be obtained either by differentiating eqs. (10) and (11) with respect to x and y, respectively, or by integrating eqs. (8) and (9) along the length of the segment. Either method leads to the following results:

$$\frac{\partial E_x}{\partial x} = \frac{\mu_0 (dI/dt)}{4\pi} \left\{ \frac{\cos\theta}{R_2} \left[\cos\theta + \frac{s_2 d \sin\theta}{d^2 + (z-z_0)^2} \right] - \frac{\cos\theta}{R_1} \left[\cos\theta + \frac{s_1 d \sin\theta}{d^2 + (z-z_0)^2} \right] \right\} \tag{18}$$

$$\frac{\partial E_y}{\partial y} = \frac{\mu_0 (dI/dt)}{4\pi} \left\{ \frac{\sin\theta}{R_2} \left[\sin\theta - \frac{s_2 d \cos\theta}{d^2 + (z-z_0)^2} \right] - \frac{\sin\theta}{R_1} \left[\sin\theta - \frac{s_1 d \cos\theta}{d^2 + (z-z_0)^2} \right] \right\} \tag{19}$$

where

$$s_1 = (x_1 - x)\cos\theta + (y_1 - y)\sin\theta \tag{20}$$

$$s_2 = (x_2 - x)\cos\theta + (y_2 - y)\sin\theta \tag{21}$$

and

$$d = (x - x_1)\sin\theta - (y - y_1)\cos\theta . \tag{22}$$

The physical meanings of s_1, s_2, l, d and θ are indicated in Fig. 2.

It is interesting to consider two special cases: a segment parallel to the x-axis and a segment parallel to the y-axis. For the former, the following expressions are obtained by substituting $\theta = 0^\circ$ in eqs. (18) and (19):

$$\frac{\partial E_x}{\partial x} = \frac{\mu_0 (dI/dt)}{4\pi} \left[\frac{1}{R_2} - \frac{1}{R_1} \right] \tag{23}$$

$$\frac{\partial E_y}{\partial y} = 0 . \tag{24}$$

It should be noted that R_1 is the distance from the point where spatial derivatives are evaluated to the segment end where the current flow starts, and R_2 is the similar distance but to the other end of the segment, *i.e.* where the current flow ends. For a segment parallel to the y-axis, substitution of $\theta = 90^\circ$ in eqs. (18) and (19) leads to the following results:

$$\frac{\partial E_x}{\partial x} = 0 \tag{25}$$

$$\frac{\partial E_y}{\partial y} = \frac{\mu_0 (dI/dt)}{4\pi} \left[\frac{1}{R_2} - \frac{1}{R_1} \right] . \tag{26}$$

Linear Coil Segment Perpendicular to the Interface

For a linear segment of the coil perpendicular to the interface and carrying a current from (x_0, y_0, z_1) to (x_0, y_0, z_2), the electric field components are obtained by integrating expressions (3) and (4) along the segment. For $\rho \neq 0$:

$$E_x = \frac{\mu_0 (dI/dt)(x - x_0)(z_1 - z_2 - R_1 + R_2)}{4\pi\rho^2} \tag{27}$$

$$E_y = \frac{\mu_0 (dI/dt)(y-y_0)(z_1-z_2-R_1+R_2)}{4\pi\rho^2} \tag{28}$$

where ρ is given by eq. (6), and

$$R_1 = \sqrt{(x-x_0)^2+(y-y_0)^2+(z-z_1)^2} \tag{29}$$

$$R_2 = \sqrt{(x-x_0)^2+(y-y_0)^2+(z-z_2)^2}. \tag{30}$$

When $\rho = 0$, *i.e.* the observation point is right below the coil-segment, both E_x and E_y vanish.

The electric-field spatial derivatives, obtained by integrating eqs. (8) and (9) along the segment, are equal to ($\rho \neq 0$)

$$\frac{\partial E_x}{\partial x} = \frac{\mu_0 (dI/dt)}{4\pi\rho^2}\left\{\frac{[(x-x_0)^2-(y-y_0)^2](z_2-z_1-R_2+R_1)}{\rho^2} + (x-x_0)^2\left[\frac{1}{R_2}-\frac{1}{R_1}\right]\right\} \tag{31}$$

$$\frac{\partial E_y}{\partial y} = \frac{\mu_0 (dI/dt)}{4\pi\rho^2}\left\{\frac{[(y-y_0)^2-(x-x_0)^2](z_2-z_1-R_2+R_1)}{\rho^2} + (y-y_0)^2\left[\frac{1}{R_2}-\frac{1}{R_1}\right]\right\} \tag{32}$$

When $\rho = 0$, they are

$$\frac{\partial E_x}{\partial x} = \frac{\partial E_y}{\partial y} = \frac{\mu_0 (dI/dt)}{8\pi}\left[\frac{1}{R_2}-\frac{1}{R_1}\right]. \tag{33}$$

Right-Angle (90°) Bends

The expressions for electric-field spatial derivatives produced by linear coil segments reveal that only the segment ends contribute to electric-field spatial derivatives. In other words, in a coil composed of several linear segments, only the bends (where current changes the direction) generate electric-field spatial derivatives.

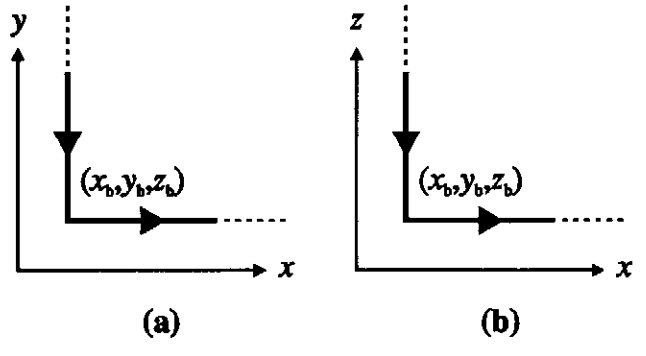

Figure 3. (a) A right-angle bend parallel to the air-tissue interface, (b) A right-angle bend perpendicular to the interface.

A 90° bend with two semi-infinite segments, one parallel to the x-axis and the other parallel to the y-axis, is shown in Fig. 3(a). Such bends are found in many stimulating coils, *e.g.* square coils parallel to the interface. The electric-field spatial derivatives produced by this bend can be obtained by substituting $R_1 = R_b$, $R_2 \to \infty$ in eq. (23) and $R_1 \to \infty$, $R_2 = R_b$ in eq. (26):

$$\frac{\partial E_x}{\partial x} = -\frac{\partial E_y}{\partial y} = -\frac{\mu_0 (dI/dt)}{4\pi R_b} \tag{34}$$

where R_b is the distance from the bend to the point of observation, and is equal

to:

$$R_b = \sqrt{(x-x_b)^2+(y-y_b)^2+(z-z_b)^2} \tag{35}$$

When $x = x_b$ and $y = y_b$, the spatial derivatives reach the following maximum or minimum values:

$$\frac{\partial E_x}{\partial x} = -\frac{\partial E_y}{\partial y} = -\frac{\mu_0 (dI/dt)}{4\pi (z_b - z)} \tag{36}$$

Figure 3(b) shows a 90°-bend with one segment parallel to the x-axis and the other parallel to the z-axis. Such bends are present in square coils perpendicular to the interface. The electric field spatial derivatives produced by this bend are obtained by substituting $R_1 = R_b$, $R_2 \to \infty$ in eq. (23) and $x_0 = x_b$, $y_0 = y_b$, $z_1 \to \infty$, $R_1 \to \infty$, $R_1 - z_1 = -z$, $z_2 = z_b$, $R_2 = R_b$ in eqs. (31) and (32):

$$\frac{\partial E_x}{\partial x} = -\frac{\partial E_y}{\partial y} = \frac{\mu_0 (dI/dt)[(x-x_b)^2 - (y-y_b)^2]}{4\pi \rho^2} \left[\frac{z_b - z - R_b}{\rho^2} + \frac{1}{R_b} \right] \tag{37}$$

where R_b is given by eq. (35) and $\rho = \sqrt{(x-x_b)^2+(y-y_b)^2}$.

For the special case of $\rho = 0$, the spatial derivatives become:

$$\frac{\partial E_x}{\partial x} = -\frac{\partial E_y}{\partial y} = -\frac{\mu_0 (dI/dt)}{8\pi (z_b - z)}. \tag{38}$$

Comparing eqs. (36) and (38), it can be seen that the peak magnitude of the spatial derivatives produced by a parallel right-angle bend is twice as large as that produced by a perpendicular right-angle bend. This explains why a square coil stimulates nerves more efficiently when it is placed parallel to the interface [Esselle and Stuchly, 1992]. It also suggests that, the relatively strong hyperpolarization produced by some parallel bends in single and multiple square coils can be significantly reduced by replacing such parallel bends with perpendicular bends. This observation has led to the three-dimensional (3D) coil design described later.

Relationship Between the Spatial Derivatives

Equations (34) and (37) show that the two orthogonal spatial derivatives of electric field, produced by a parallel or perpendicular 90° bend, are related in the following manner:

$$\frac{\partial E_y}{\partial y} = -\frac{\partial E_x}{\partial x}. \tag{39}$$

It can be shown that this relationship is true for the spatial derivatives produced by any coil of an arbitrary shape and orientation [Esselle and Stuchly, 1992].

Quadruple Coils

Several quadruple coils have been proposed for nerve stimulation [Roth *et al.*, 1990b, Esselle and Stuchly, 1991]. Although there are substantial differences between them, all the quadruple coils have several common advantages over single and double coils when used for stimulation of long nerves. They almost always produce only one stimulation spot (the primary depolarization peak) in a well-defined location (right below the coil centre). Their

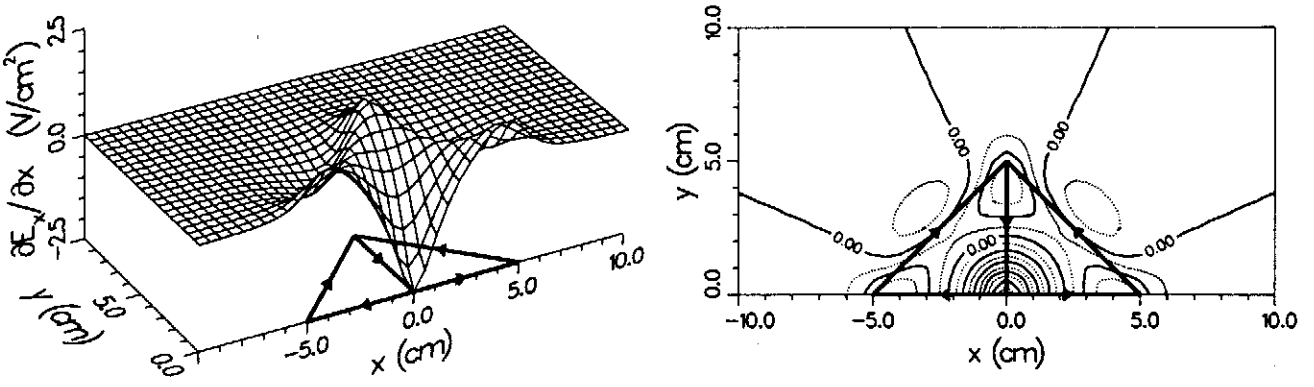

Figure 4. Plots of $\partial E_x/\partial x$ in a plane 1-cm below a QT coil. Each triangular section is 5-cm long, has 10 turns, and carries a current rising at 100 A/μs.

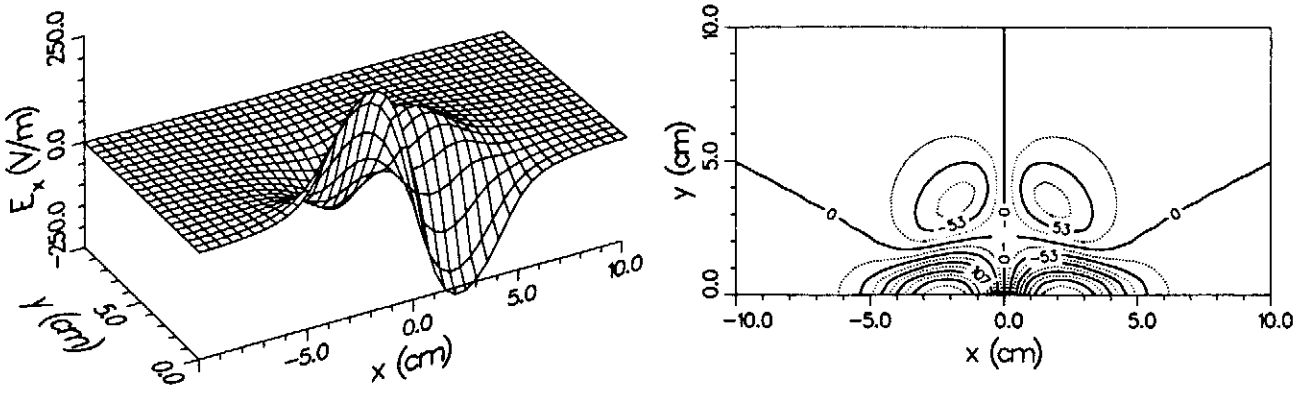

Figure 5. Plots of E_x in a plane 1-cm below a QT coil. Each triangular section is 5-cm long, has 10 turns, and carries a current rising at 100 A/μs.

secondary depolarization peaks and hyperpolarization peaks are relatively weak (< 50% of primary depolarization peak). If the time rate of change of current and the total number of turns are constant, properly designed quadruple coils will create the same peak spatial derivative of the electric field as their single counterparts. However, the inductance of a quadruple coil is lower than that of a single coil with the same total number of turns, and therefore, the quadruple coil draws a larger current and produces a stronger peak spatial derivative of electric field when used with a given stimulator (for a fixed stimulator voltage).

The electric field and its spatial derivatives produced by quadruple Focalpoint^{TM} coils [Roth *et al.*, 1990b] and quadruple square (QS) coils [Esselle and Stuchly, 1992] have been analyzed previously. Two other coil configurations are discussed here. Figure 4 shows the electric-field spatial derivative ($\partial E_x/\partial x$) produced by a

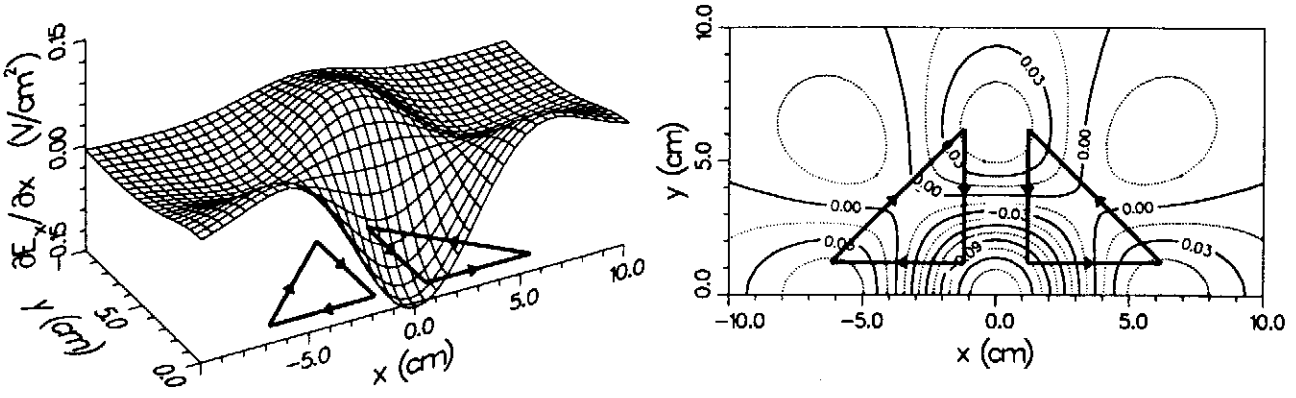

Figure 6. Plots of $\partial E_x/\partial x$ in a plane 4-cm below a QT coil. Each triangular section is 5-cm long, has 10 turns, and carries a current rising at 100 A/μs. Gap between sections (s) = 2.4 cm.

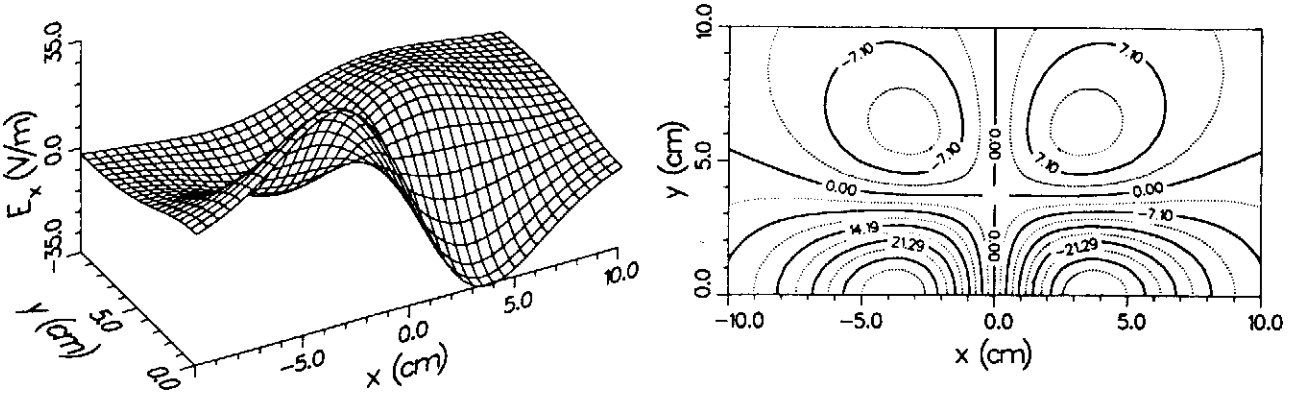

Figure 7. Plots of E_x in a plane 4-cm below a QT coil. Each triangular section is 5-cm long, has 10 turns, and carries a current rising at 100 A/μs. Gap between sections (s) = 2.4 cm.

quadruple triangular (QT) coil, in a relatively shallow plane inside tissue 1-cm below the coil. These and the following 3D and contour plots are symmetrical about the x-axis, and therefore only the $y \geq 0$ region of the plots is shown. In all contour plots, the contour interval is equal to one tenth the peak magnitude ($|\partial E_x/\partial x|_{peak}$ or $|E_x|_{peak}$). The x-component of the electrical field (E_x) produced by the QT coil is shown in Fig. 5. Figures 6 and 7, respectively, show $\partial E_x/\partial x$ and E_x produced by the same coil, but in a deeper plane 4-cm below the coil. The four triangular sections have been optimally spaced for maximum $|\partial E_x/\partial x|_{peak}$. The distance between turns in each triangle has been neglected in these calculations.

For a 10-cm x 10-cm QS coil, the relative peak hyperpolarization level (RPHL, defined as the ratio of the greatest positive value of $\partial E_x/\partial x$ and the greatest negative value of it) in a plane 1-cm below the coil is 47%

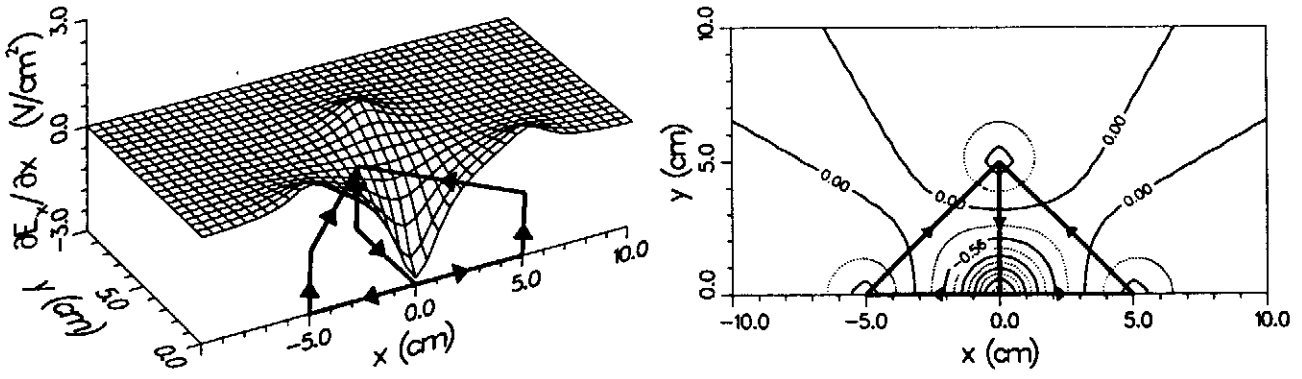

Figure 8. Plots of $\partial E_x/\partial x$ in a plane 1-cm below a 3D coil. Each section is 5-cm long and 2-cm high, has 10 turns, and carries a current rising at 100 A/μs.

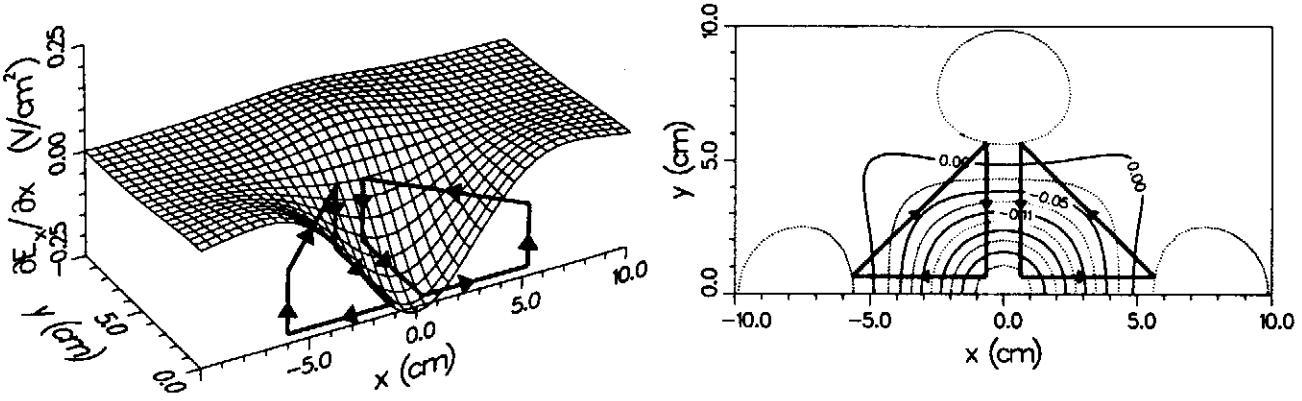

Figure 9. Plots of $\partial E_x/\partial x$ in a plane 4-cm below a 3D coil. Each section is 5-cm long and 2-cm high, has 10 turns, and carries a current rising at 100 A/μs. Gap between sections (s) = 1.3 cm.

[Esselle and Stuchly, 1992]; for a QT coil, it is 40% (Fig. 4). In both cases, the primary hyperpolarization spots as well as the secondary depolarization spots are created by additional bends in the coil that are parallel to the interface. Since these bends are not necessary for creation of the primary stimulation spot (at $x=0$, $y=0$), it is convenient to replace these parallel bends with perpendicular bends that produce smaller spatial derivatives. A three-dimensional (3D) coil obtained by modifying the QT coil, and its $\partial E_x/\partial x$ in a plane 1-cm below its bottom, are shown in Fig. 8. For these calculations, the coil height was assumed to be 2 cm, which results in a RPHL of 24%. This level can be further reduced by increasing the coil height, but at the expense of increased coil inductance and hence reduced coil current. Figure 9 shows the electric field spatial derivatives in a plane 4-cm below the coil. Again, coil sections are spaced for maximum $|\partial E_x/\partial x|_{peak}$.

III. COIL INDUCTANCE

In practical magnetic nerve stimulators, the time-rate of change of coil current strongly depends on the coil inductance, as expressed in eq. (1). Inductance can be calculated using a general equation for an arbitrary thin-wire coil given by Ramo *et al.* [1965], and applying it to coil segments as detailed in the Appendix. Analytical expressions derived therein have been used to calculate inductances of several square, QS, QT and 3D coils. Representative results are shown in Fig. 10 and Table I. In Fig. 10, the inter-turn distance (d) is also taken into account, assuming that the turns are stacked to form a single-layer tube, as shown in Fig. 11.

Table I. The inductance (L) and the peak spatial derivative of electric field per unit voltage (S). The square coil is 5-cm long and has 4 turns. All quadruple coils consist of 5-cm-long single-turn sections. Wire radius is 0.9 mm. Depth is measured from the bottom of the coil; d is the distance between turns; s is the gap between sections; b is the height of the 3D coil.

Coil type and parameters	Inductance L (μH)	S at 1-cm depth (m^{-2})	S at 4-cm depth (m^{-2})
Square ($d=0$)	2.03	14.7	1.3
QS ($s=0$)	0.63	47.1	4.0
QS ($s=1.6$ cm)	0.54	32.9	5.0
QT ($s=0$)	0.44	57.1	2.5
QT ($s=2.4$ cm)	0.37	28.5	4.3
3D ($s=0$, $b=2$ cm)	0.67	42.1	3.7
3D ($s=1.3$ cm, $b=2$ cm)	0.54	35.5	4.9

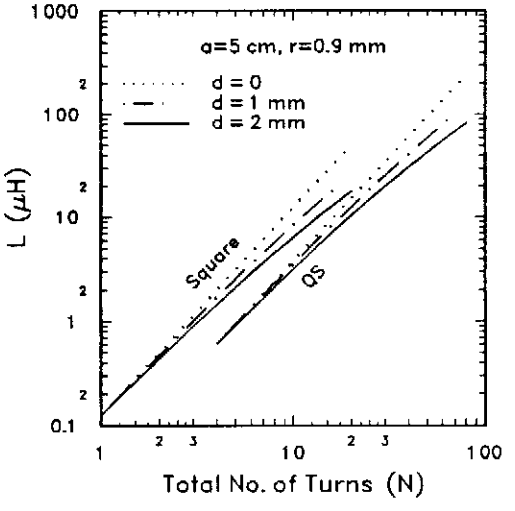

Figure 10. Inductance of square and QS coils versus number of turns. The inter-turn distance is d. Square coil is 5 cm x 5 cm; QS coil has four such square sections. Wire radius (r) = 0.9 mm, gap (s) = 0.

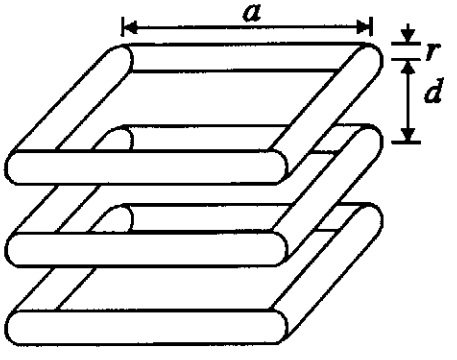

Figure 11. A square coil, or a section of a QS coil. Wire turns are stacked to form a single-layer tube.

With zero inter-turn distance, the inductance of any coil should increase according to the square of the number of turns. A finite inter-turn distance results in lower inductance. The inductance of a QS coil is 1.7 to 3.3 times less than that of a square coil with the same total number of turns. This is when the gap (s) between the four square sections in the coil is zero, as assumed in Fig. 10; otherwise, the inductance is even less. Table I shows the inductance of several 4-turn coils. In general, the QT coil has lower inductance than a QS coil, but the 3D coil has a higher inductance unless the coil height is very small.

IV. COIL OPTIMIZATION AND COMPARISON

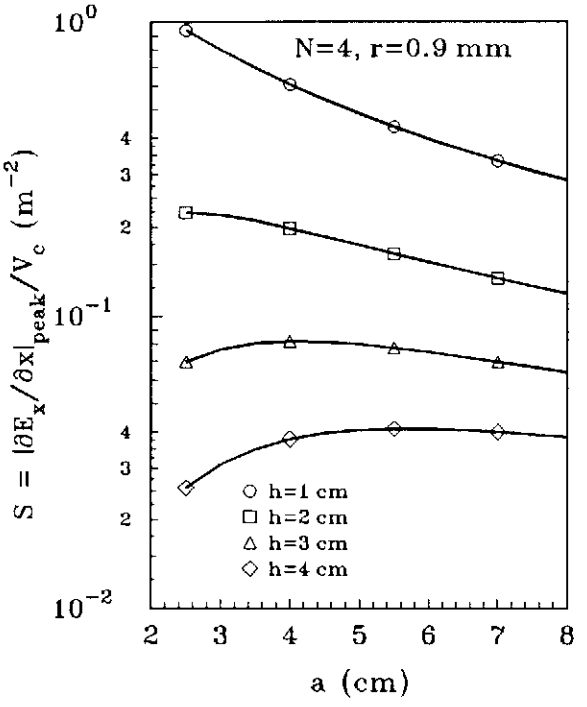

Figure 12. The peak electric-field spatial derivative per unit voltage (S) versus the length of one square section (a), for 4-turn QS coils. h is the depth of the nerve measured from the coil.

First, we search for the optimum size of a coil assuming that its shape, wire radius, number of turns and the voltage applied across the coil terminals (V_c) are fixed. The peak electric field and the peak electric-field spatial derivative the coil produces at a given depth in tissue depend on the coil size. Using the methods described in Sections II and III, peak electric-field spatial derivative per unit voltage,

$$S = \frac{|\partial E_x/\partial x|_{peak}}{V_c} = \frac{|\partial E_x/\partial x|_{peak}}{L\,(dI/dt)} \qquad (40)$$

can be calculated for different coil sizes. Results for QS coils are shown in Fig. 12. For a given depth of the nerve (h), there is an optimum QS coil size that gives maximum S. However, for shallow nerves, the optimum QS coil size is too small for practical realization [Cohen and Cuffin, 1991]. Not only are they difficult to wind, but also have low inductance, draw a heavy current and require large capacitor banks. On the other hand, optimum QS coils are practical and useful for deep-nerve stimulation.

Next, we alter the shape of, and the gap between, the four sections of a quadruple coil, keeping the size approximately constant. The last two columns in Table I give the value of S for several useful coils at 1-cm and 4-cm depths. All coils have the same characteristic dimension (length of one section) of 5 cm. It can be seen that as far as the strength of the stimulus is concerned, unspaced QT coils are preferred for shallow nerves, and spaced QS or 3D coils are preferred for deep nerves.

In addition to the parameter S, there are other factors to be considered before choosing a coil for magnetic nerve application. The rate at which the peak value of $|\partial E_x/\partial x|$ decreases with depth is critical when stimulating deep-lying nerves. Figure 13 shows this drop for several quadruple coils. It can be seen that all spaced coils have approximately equal drop-rates. Unspaced coils have higher drop-rates, the QT having the highest. Figure 14 shows how the peak value of E_x decreases with depth. Again, the QT coil has the highest drop-rate.

The focality of a coil is determined by the size of the stimulation region. When the peak stimulus is 10% higher than the threshold stimulus, the stimulation region is marked by the 90% (of $-|\partial E_x/\partial x|_{peak}$) contour. The width ($\Delta X$) of the 90%-contour is plotted as a function of nerve depth (distance from the coil) in Fig. 15. In

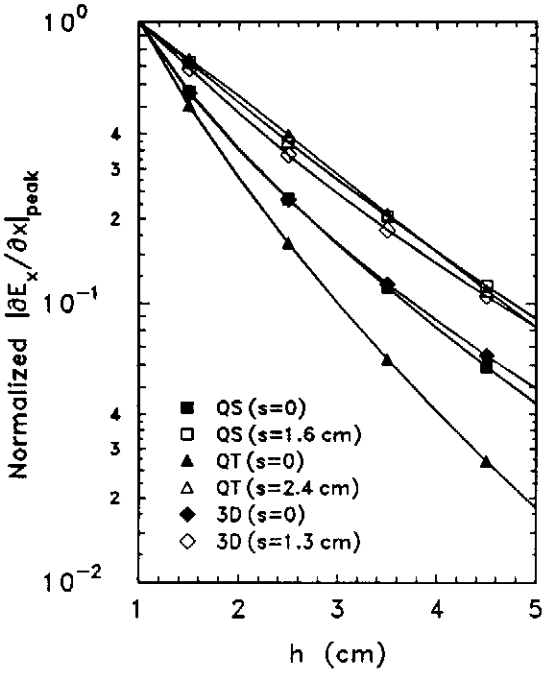

Figure 13. Peak electric-field spatial derivative normalized to value at 1-cm depth, versus depth (h) measured from the bottom of the coil. s is the gap between the four sections. N = 40, d=0.

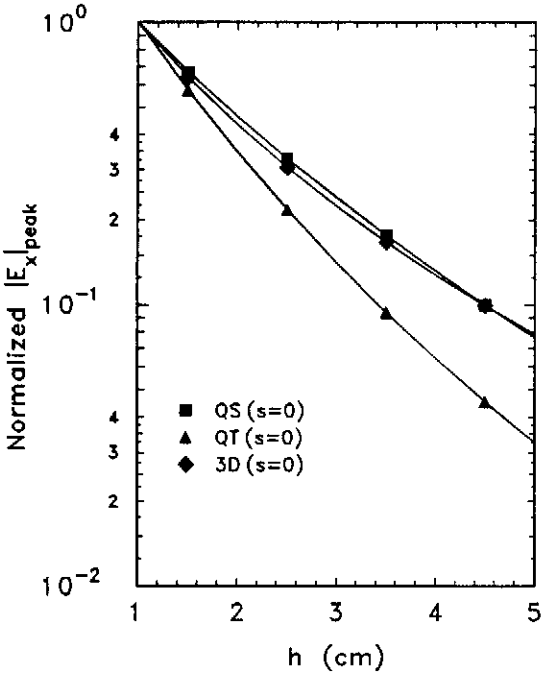

Figure 14. Peak electric field normalized to value at 1-cm depth, versus depth (h) measured from the bottom of the coil. There is no gap between the four sections. No. of turns = 40. Inter-turn distance is neglected.

general, QT coils are more focal than QS and 3D coils. Unspaced coils are usually more focal than spaced coils, but the difference is trivial in deep-nerve stimulation.

In practice, the coil is usually placed in such a position that the stimulation region (spot) coincides with the nerve to be stimulated. However, some other nerves that are at the secondary depolarization peaks of the coil may also be stimulated unintentionally if they have sufficiently lower stimulation thresholds. Also some other nerves may be hyperpolarized at the hyperpolarization peaks of the coil. Since the secondary depolarization peaks and hyperpolarization peaks of quadruple coils are equal in magnitude, the severity of both these potentially harmful effects can be expressed by a single parameter: the relative peak hyperpolarization level (RPHL) defined before (See sub-section: *Quadruple Coils*). Figure 16 shows the RPHL of quadruple coils; it is 100% for single and double coils. At all depths, 3D coils have significantly lower RPHL; for deep nerves it is less than half of the RPHL produced by other coils.

V. CONCLUSIONS

In stimulation of nerves with pulsed magnetic field several parameters of the stimulating coil have to be considered to produce effective stimulation of a desired nerve. For long, straight nerves the activation function is the spatial derivative of the electric field along the neuronal axis. This derivative depends on the coil design, shape and location with respect to the nerve. Ideally, the coil should produce a small region at a desired location of the nerve where the stimulus produces nerve depolarization. In practice, more than one region of depolarization as well as regions of hyperpolarization are produced. Furthermore, for a given stimulator, having a bank of capacitors that are charged to a given voltage, the stimulus is inversely proportional to the coil inductance.

Simplified analyses described here, that heavily rely on analytical solutions in addition to simple numerical computations, provide tools for coil optimization and comparison. This can lead to a selection of the best coil geometry and location for selective stimulation of a desired long nerve. Furthermore, the physical insight gained from this analysis should prove useful for more complex numerical analyses of tissue models better reflecting tissue geometry and heterogeneous electrical properties.

Quadruple coils of various shapes emerged from our evaluation as the optimal coils for stimulation of long

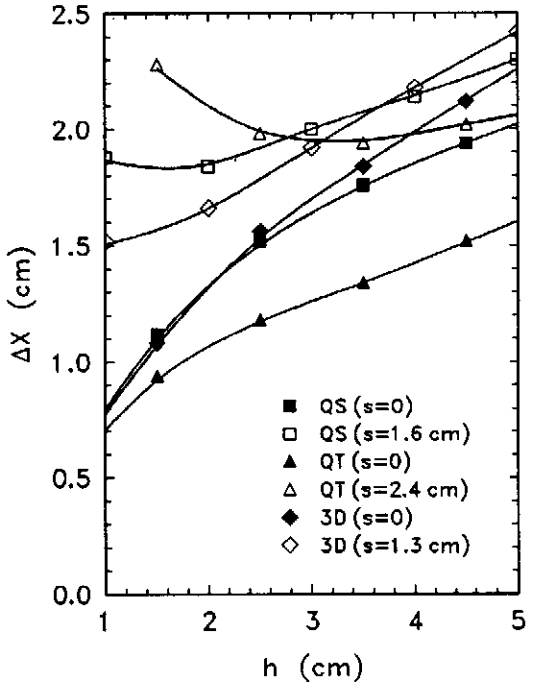

Figure 15. The size of the stimulation spot versus depth (h) measured from the bottom of the coil. The gap between the four coil sections is s.

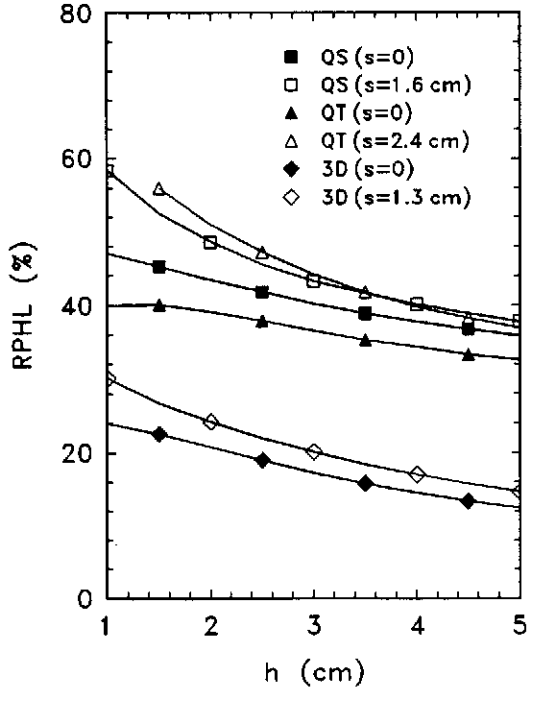

Figure 16. Relative peak hyperpolarization level versus depth (h) measured from the bottom of the coil. The gap between the four coil sections is s.

straight nerves.

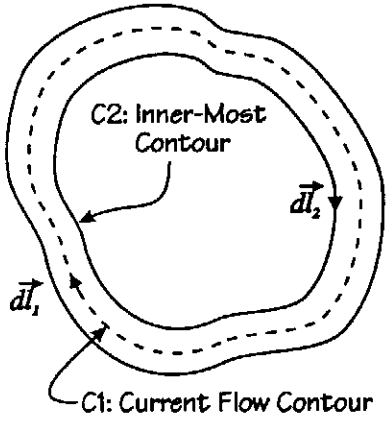

Figure A1. A thin-wire coil of arbitrary shape. Current is assumed to be concentrated along the centre-line.

VI. APPENDIX

For a general thin-wire coil shown in Fig. A1, inductance is given by [Ramo *et al.*, 1965]:

$$L = \frac{\mu_o}{4\pi} \oint_{C_1} \oint_{C_2} \frac{d\vec{l}_1 . d\vec{l}_2}{d} \qquad \text{(A1)}$$

where C_1 is the contour along the centre-line of the wire, C_2 is the inner-most contour, $d\vec{l}_1$ is an elemental vector on C_1, located at (x_1, y_1, z_1), $d\vec{l}_2$ is an elemental vector on C_2, located at (x_2, y_2, z_2), and

$$d = \sqrt{(x_1-x_2)^2+(y_1-y_2)^2+(z_1-z_2)^2}.$$

It should be noted that eq. (A1) is valid only for coils composed of relatively thin wires where the current can be assumed to be concentrated along the centre-line.

For an arbitrarily-shaped coil, evaluation of eq. (A1) requires two numerical integrations. However, for coils composed of linear segments, at least one of the contour integrations can be done analytically. In this case, it is desirable to break the total inductance (L) into partial inductances due to each pair of linear segments. If the partial inductance due to i^{th} and j^{th} segment-pair as a result

of the current in the j[th] segment is L_{ij},

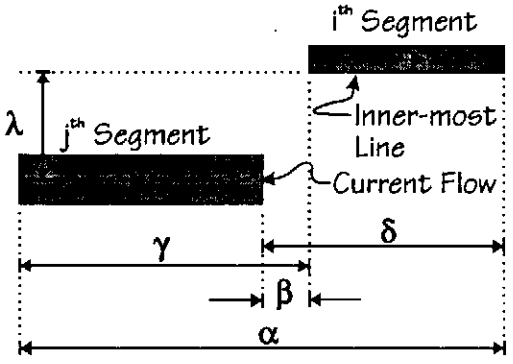

Figure A2. Two linear parallel segments of a coil.

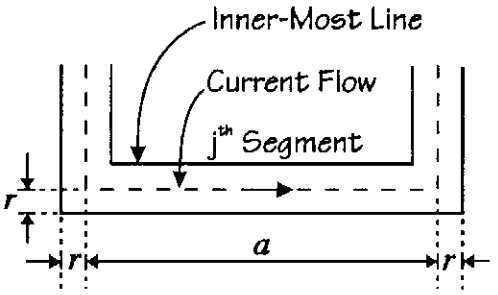

Figure A3. A segment of a square or QS coil.

$$L = \sum_{i=1}^{N_s} \sum_{j=1}^{N_s} L_{ij} \tag{A2}$$

where N_s is the number of segments in the coil.

When i[th] and j[th] segments are perpendicular to each other, the dot product in eq. (A1) leads to $L_{ij} = 0$. When the centre-line of the j[th] segment is parallel to the inner-most line of the i[th] segment, as shown in Fig. A2, both contour integrations can be performed analytically, giving [Ramo *et al.*, 1965]:

$$\begin{aligned} L_{ij} = (\mu_o/4\pi)\,[\, & \alpha \ln(\alpha+\sqrt{\alpha^2+\lambda^2}) - \sqrt{\alpha^2+\lambda^2} + \beta \ln(\beta+\sqrt{\beta^2+\lambda^2}) - \sqrt{\beta^2+\lambda^2} \\ & - \gamma \ln(\gamma+\sqrt{\gamma^2+\lambda^2}) + \sqrt{\gamma^2+\lambda^2} - \delta \ln(\delta+\sqrt{\delta^2+\lambda^2}) + \sqrt{\delta^2+\lambda^2}\,] \end{aligned} \tag{A3}$$

where α, β, γ, δ and λ are the dimensions shown in Fig. A2. The above expression assumes that both segments carry current in the same direction; the sign of L_{ij} should be reversed otherwise. As a special case, eq. (A3) can be used to evaluate L_{jj}, the self-contribution from the j[th] segment. For example, L_{jj} for the segment shown in Fig. A3 can be obtained by substituting $\alpha = a-r$, $\beta = -a+r$, $\gamma = r$, $\delta = -r$ and $\lambda = r$ in eq. (A3), which results in

$$L_{jj} = \frac{\mu_o}{4\pi}\left\{(a-r)\ln\left[\frac{a-r+\sqrt{(a-r)^2+r^2}}{r-a+\sqrt{(a-r)^2+r^2}}\right] - 2\sqrt{(a-r)^2+r^2} - r\ln\left(\frac{\sqrt{2}+1}{\sqrt{2}-1}\right) + 2\sqrt{2}r\right\}. \tag{A4}$$

The calculation of L_{ij} due to two linear segments, which are parallel to the x-y plane but not parallel to each other (Fig. A4), can be also be done without numerical integration. The inner-most line of the i[th] segment extends from A $\equiv (x_1^i, y_1^i, z_1^i)$ to B $\equiv (x_2^i, y_2^i, z_1^i)$, and the centre-line of the j[th] segment extends from C $\equiv (x_1^j, y_1^j, z_1^j)$ to D $\equiv (x_2^j, y_2^j, z_1^j)$. Lengths of AB and CD, denoted by l^i and l^j, are given by

$$l^i = \sqrt{(x_2^i-x_1^i)^2 + (y_2^i-y_1^i)^2} \tag{A5}$$

$$l^j = \sqrt{(x_2^j-x_1^j)^2 + (y_2^j-y_1^j)^2} \tag{A6}$$

and their direction cosines are given by

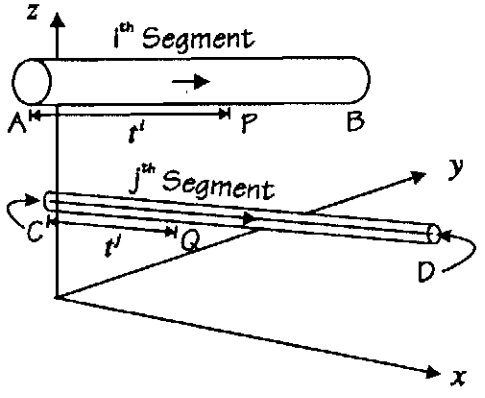

Figure A4. Two linear segments parallel to the x-y plane.

$$m^i = \frac{x_2^i - x_1^i}{l^i}, \qquad m^j = \frac{x_2^j - x_1^j}{l^j} \tag{A7}$$

$$n^i = \frac{y_2^i - y_1^i}{l^i}, \qquad n^j = \frac{y_2^j - y_1^j}{l^j} \tag{A8}$$

For two generic points: P $\equiv (x^i, y^i, z^i)$ on AB, at a distance of t^i from A, and Q $\equiv (x^j, y^j, z^j)$ on CD, at a distance of t^j from C, the following relationships apply:

$$x^i = x_1^i + m^i t^i, \qquad x^j = x_1^j + m^j t^j \tag{A9}$$

$$y^i = y_1^i + n^i t^i, \qquad y^j = y_1^j + n^j t^j \tag{A10}$$

$$z^i = z_1^i, \qquad z^j = z_1^j \tag{A11}$$

According to eq. (A1), the partial inductance is given by

$$L_{ij} = \frac{\mu_0 (m^i m^j + n^i n^j)}{4\pi} \int_0^{l^j} \int_0^{l^i} \frac{dt^i\, dt^j}{\sqrt{(x^i - x^j)^2 + (y^i - y^j)^2 + (z^i - z^j)^2}}. \tag{A12}$$

The first integration in the above expression with respect to t^i is straightforward, but the resulting general analytical expression is fairly lengthy. This expression can be significantly simplified in some special cases, such as the segment-pairs in QT and 3D coils. The second integration, with respect to t^j, can also be done analytically, using the following integral:

$$\begin{aligned} \int \ln[p t^j + q + \sqrt{t^{j2} + r t^j + s}]\, dt^j \;=\; & -\frac{r}{2p^2} - t^j - \frac{2\Delta}{p^2 - 1} \tan^{-1}\left[\frac{q + r/2 + (1+p)(t^j + \Phi)}{\Delta}\right] \\ & - \frac{q - r/2}{p - 1} \ln\left(\frac{r}{2} + t^j + \Phi\right) + t^j \ln(q + p t^j + \Phi) \\ & + \frac{pq - r/2}{p^2 - 1} \ln\left\{2s - \frac{r^2}{2} + (r + 2t^j + 2\Phi)\left[q + \frac{r}{2} + (1+p) t^j\right]\right\} \end{aligned} \tag{A13}$$

where

$$\Delta = \sqrt{(p^2 - 1)(q^2 - s) - \left(pq - \frac{r}{2}\right)^2} \tag{A14}$$

and

$$\Phi = \sqrt{t^{j2} + r t^j + s}. \tag{A15}$$

The above integral as well as many other analytical expressions were obtained using the symbolic computation capability in the Mathematica® software package [Wolfram, 1991].

VII. REFERENCES

Barker A.T., Freeston I.L., Jalinous R. and Jarratt J.A. (1986) Clinical evaluation of conduction time measurements in central motor pathways using magnetic stimulation of the human brain. *Lancet*, i:1106.

Barker A.T., Freeston I.L., Jalinous R. and Jarratt J.A. (1987) Magnetic stimulation of the human brain and peripheral nervous system: an introduction and the results of an initial clinical evaluation. *J. Neurosurgery*,

20:100-109.

Basser P.J. and Roth B.J. (1991) Stimulation of a myelinated nerve axon by electromagnetic induction. *Med. & Biol. Eng. Comput.*, 29:261-268.

Branston N.M. and Tofts P.S. (1991) Analysis of the distribution of currents induced by a changing magnetic field in a volume conductor. *Phys. Med. Biol.*, 36:161-168.

Chokroverty S. (1990) *Magnetic stimulation in clinical neurophysiology.* Butterworks Publishing, Boston, MA.

Cohen D. and Cuffin B.N. (1991) Developing a more focal magnetic stimulator. Part I: some basic principles. *J. Clin. Neurophysiol.*, 8:102-111.

Cohen L.G., Roth B.J., Nilsson J., Dang N., Panizza, M., Bandinelli S., Friauf W. and Hallett, M. (1990) Effect of coil design on delivery of focal magnetic stimulation. Technical Considerations. *Electroencephal. Clin. Neurophysiol.*, 75:350-357.

Cohen L.G., Roth B.J., Wassermann E.M., Topka H., Fuhr P., Schultz J. and Hallen M. (1991) Magnetic stimulation of the human cerebral cortex, an indicator of reorganization in motor pathways in certain pathological conditions. *J. Clin. Neurophysiol.*, 8:56-65.

Esselle K.P. and Stuchly M.A. (1992) Neural stimulation with magnetic fields: analysis of induced electric fields. *IEEE Trans. Biomed. Eng.*, 39:693-700.

Geddes L.A. (1991) History of magnetic stimulation of the nervous system. *J. Clin. Neurophysiol.*, 8:3-9.

Grandori F. and Ravazzani P. (1991) Magnetic stimulation of the motor cortex - theoretical considerations. *IEEE Trans. Biomed. Eng.*, 38:180-191.

Maccabee P.J., Amassian V.E., Cracco R.Q., Cracco J.B., Eberle L. and Rudell A. (1991) Stimulation of the human nervous system using magnetic coil. *J. Clin. Neurophysiol.*, 8:38-55.

Murray N.M.F. (1991) Magnetic stimulation of cortex: clinical applications. *J. Clin. Neurophysiol.*, 8:66-76.

Ramo S., Whinnery J.R. and Van Duzer T. (1965) *Fields and Waves in Communication Electronics*. John Wiley & Sons, New York, NY.

Roth B.J., Cohen L.G., Hallett M., Friauf W. and Basser P.J. (1990a) A theoretical calculation of the electric field induced by magnetic stimulation of a peripheral nerve. *Muscle & Nerve*, 13:734-741.

Roth B.J., Turner R., Cohen L.G. and Hallet M. (1990b) New coil design for magnetic stimulation with improved focality. *Movement Disorders*, 5 (Suppl. 1):32.

Roth B.J., Saypol J.M., Hallett M. and Cohen L.G. (1991a) A theoretical calculation of the electric field induced in the cortex during magnetic stimulation. *Electroencephal. Clin. Neurophysiol.*, 81:47-56.

Roth B.J., Cohen L.G. and Hallett M. (1991b) The electric field induced during magnetic stimulation. *Electroencephal. Clin. Neurophysiol.* (Suppl. 43):268-278.

Wolfram S. (1991) *Mathematica: a system for doing mathematics by computer.* Addison-Wesley Publishing, Redwood City, CA.